

A Review on the Dynamics of Water

Milton T. Sonoda, Ney H. Moreira, Leandro Martínez, Frank W. Favero,
Sérgio M. Vechi, Lucimara R. Martins, and Munir S. Skaf

Instituto de Química, Universidade Estadual de Campinas, Cx. P. 6154, Campinas, SP, 13084-971, Brazil

Received on 17 October, 2003.

We present a review on the intermolecular dynamics of liquid aqueous systems focusing mainly on Molecular Dynamics simulation work that has been carried out at the State University of Campinas in recent years. Emphasis is given on simulation results that are more directly related to modern experimental spectroscopic measurements.

1 Introduction

Water is by far the most important, most ubiquitous, most studied, and yet one of the least understood liquids on Earth. The strength and high directionality (anisotropy) of the intermolecular interactions in water lead to highly peculiar thermodynamic and structural properties [1-4]. The nature of the intermolecular interactions allied to water's low molecular weight and small moments of inertia, allow for a complex pattern of intermolecular force fluctuations in both length and time scales, promoting a dynamical behavior that is unique to water[3, 4]. At the heart of water's intriguing behavior lies the network of hydrogen (H) bonding. In addition, manifestations of inherently quantum mechanical effects on water's macroscopic behavior brings in an additional degree of challenge, and fascination, to this field of research[5].

The intermolecular dynamics of liquid water has long been subject of intense experimental and theoretical research. Numerous experimental studies have been reported on the dynamics of this liquid using a variety of different techniques, including microwave dielectric relaxation[6], far-infrared[7], Raman[8] and light scattering spectroscopies[9], NMR[10], and small angle neutron scattering[11] in the last two or three decades. More recently, new experimental developments based on ultrafast laser techniques have made it possible to investigate intermolecular dynamical processes of water at much shorter timescales with substantially higher level of detail. Among these, terahertz spectroscopy[12] and nonlinear optical methods such as Raman echo[13] and optical Kerr effect (OKE)[14] spectroscopies stand out for providing remarkably valuable information directly in the time domain.

Parallel to these developments, advances in molecular dynamics (MD) computer simulations have markedly enriched our views on the dynamics of water, both at ambient and extreme conditions of temperature and pressure[3, 4]. A variety of MD simulation studies have been performed on liquid water aiming to understand different aspects of its dynamics by means of interaction potentials of distinct com-

plexity. In particular, detailed simulation analyses have been reported for the dielectric relaxation, depolarized Raman or light scattering, time resolved fluorescence spectroscopy[3], and nonlinear optical Kerr response for bulk phases[15], as well as second harmonic generation and vibrational sum frequency[16] signals for studying interfacial systems more specifically. In this work, we present a nonpretentious review on the dynamics of liquid water and other aqueous systems that focuses especially on our own recent work with an emphasis on simulations of physical observables of spectroscopic relevance. Some of the results presented here have not heretofore been published. We shall not discuss any aspects related to techniques of MD simulation and will not review the numerous Hamiltonian models available for water nor the description they provide for the physicochemical properties of the fluid. The purpose here is to provide an overall physical picture for the underlying water dynamics within different contexts, as obtained from MD simulations.

The paper evolves from a tutorial review on the fundamental characteristics of the dynamics of liquid water described in terms of single-particle motions to an abridged presentation of MD studies of distinct spectroscopic properties of selected aqueous systems including: i) Dielectric relaxation and far-infrared spectroscopies of water, water-methanol and water-dimethylsulfoxide (DMSO) binary mixtures, and supercritical water; ii) Ultrafast time-resolved spectroscopy of coumarin dyes in water and water-DMSO mixtures, and of excess hydrated electrons; iii) Nonlinear optical spectroscopy of water; iv) Vibrational dephasing of the squarate anion in water; and v) Water near interfaces. The paper concludes with a brief description of the role of water in the dissociation of the retinoic acid from its nuclear hormone receptor.

2 Single-particle dynamics

The seminal MD simulations of Raham and Stillinger some thirty years ago provided the first look into the molecular motions of liquid water[17]. Detailed knowledge on the

translational motions of individual atoms or the molecule as a whole, as well as the molecular rotational motions is most commonly described in terms of the time correlation functions (TCF), $C_{\mathcal{O}}(t) = \langle \mathcal{O}(t) \cdot \mathcal{O}(0) \rangle / \langle |\mathcal{O}(0)|^2 \rangle$, with the dynamical variable $\mathcal{O}(t)$ being the linear velocities of individual atoms (v_O, v_H) or the molecular angular velocity components ($\Gamma_{x,y,z}$). Linear and angular velocity TCFs obtained from MD simulations using the SPC/E model[18] are depicted in Fig.1 (upper panels) along with their frequency spectra obtained from the cosine Fourier transforms (lower panels). The dynamics we see here refer to intermolecular motions only. Intramolecular vibrational motions are not portrayed in Fig.1 because the SPC/E model lacks internal degrees of freedom. Notice how the TCFs rapidly converge to vanishing amplitudes within 100 – 500 fs. This gives an idea of how fast are the collision rates in liquid water. The short-time dynamics of the O and H atoms are suggestive of damped oscillatory motions and result from the interactions (“collisions”) with neighboring molecules. These features resemble somewhat the dynamics of solids. The translational velocity TCF of the O atoms exhibits a negative portion due to the back scattering motions of the molecule inside the H-bonded cage of neighbors. The dynamics of the H atoms in this time scale is much faster because of their small masses. Translational motions of H atoms is highly correlated to rotations of the molecule as a whole around the center of mass and this is why the $C_{vH}(t)$ and $C_{\Gamma}(t)$ functions are similar. The $C_{\Gamma}(t)$ TCFs indicate very clearly the existence of small amplitude, hindered or damped rotational oscillations known as librations. The librational period lies between 20 and 40 fs. These fast rotational oscillations appear so prominently in water because of the small moments of inertia and the existence of high molecular torques due to H-bonding restoring forces[3, 17]. The differences observed between the angular velocity components correlate with the magnitude of the moments of inertia, $I_{xx} = 1.0 \times 10^{-47}$ kg/m² (parallel to the HH vector), $I_{yy} = 1.9 \times 10^{-47}$ kg/m² (main symmetry axis), and $I_{zz} = 2.9 \times 10^{-47}$ kg/m² (normal to plane): Smaller moment means faster rotation about the corresponding principal axis.

The characteristic frequencies associated with these motions are reflected in the Fourier spectra. The hindered translational motions of the molecule (O atom) inside the cage of neighbors have a main frequency component around 250 cm⁻¹. A small shoulder can be seen around 60 cm⁻¹. The spectral characteristics of the librations consist of a broad band between 400 and 1000 cm⁻¹, which is composed by the librations around the y and z axes peaked at ~ 600 cm⁻¹ and around the x axis, peaked near 850 cm⁻¹. The large width of the librational band reveals the structural inhomogeneity of the H-bond network and the importance of

thermal fluctuations at ambient conditions. These molecular motions can be directly or indirectly captured by a variety of spectroscopic measurements.

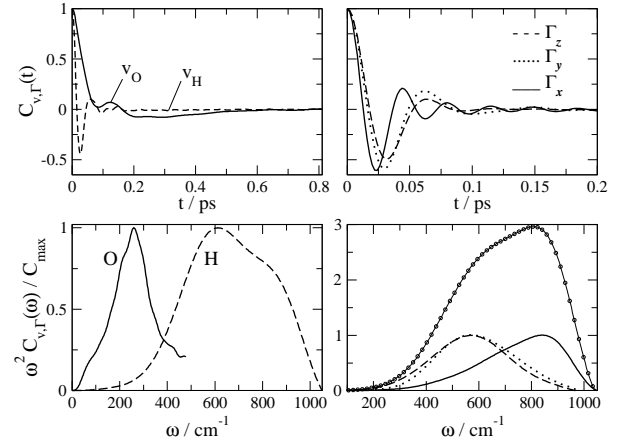


Figure 1. Normalized time correlation functions for the linear and angular velocities of water obtained from MD simulations using the SPC/E model and the corresponding frequency spectra. a) TCFs for the velocities of the oxygen and hydrogen atoms; b) TCFs for angular velocities; c) Frequency spectra for the atom velocity TCFs; Frequency spectra for the angular velocity TCFs (the line with symbols is the sum of the individual spectra).

3 Dielectric Response

Dielectric relaxation techniques are among the oldest and most popular methods to extract information about the system’s dynamics over a wide range of frequency values. The keen interest in the dielectric behavior of polar liquids is largely due to the fact that these properties are essential to characterize the liquid as a reactional medium for chemical processes involving ionic or polar species[19]. Dielectric properties such as dielectric constants, dielectric relaxation times, frequency dependent far infrared (FIR) absorption coefficients, and longitudinal dielectric relaxation times are key ingredients to the description of a variety of physicochemical phenomena, specially solvation dynamics and charge transfer reactions[20]. In very simple physical terms, the dielectric response relies on the absorption of radiation by matter that occurs when the frequency of the incident radiation matches the dynamical fluctuations of the sample’s total dipole moment. Within a linear response framework, the frequency dependent complex dielectric permittivity is related to the Fourier transform of the system’s collective dipole moment TCF:

$$\epsilon(\omega) - \epsilon_{\infty} = \frac{1}{3V k_B T \epsilon_0} \left[\langle |\mathbf{M}(0)|^2 \rangle + i\omega \int_0^{\infty} dt \langle \mathbf{M}(t) \cdot \mathbf{M}(0) \rangle e^{i\omega t} \right]. \quad (1)$$

Such time correlation functions can be computed from lengthy molecular trajectories generated from an MD simulation and then Fourier transformed to yield $\epsilon(\omega)$. One of the earliest and most complete set of MD simulations aimed at the dielectric response of water is reported by Neumann[21] using the TIP4P water model[22]. The real and imaginary parts of $\epsilon(\omega)$ as function of frequency up to 2×10^{14} Hz ($\sim 1000 \text{ cm}^{-1}$) are depicted in Fig.2 by the upper and lower curves. Solid and dotted lines correspond, respectively, to simulation and experimental results, obtained from different spectroscopic measurements[6, 7]. Starting from upper frequencies, one notices in $\text{Im } \epsilon(\omega)$ sharp absorption features due to the internal molecular vibrations, followed by a broader band around 10^{14} Hz which is due to the intermolecular librational motions. Next to it, at $\omega \sim 3 \times 10^{13}$ Hz ($150\text{-}200 \text{ cm}^{-1}$) there is another resonance which it not captured by the TIP4P simulations. At much lower frequencies, a broad absorption band appears in the microwave region resulting from the rotational-diffusion reorientational motions of the water molecules with a typical dielectric relaxation or Debye time around 10 ps. This dynamics is well described by the simulations, although not apparent in the results shown in Fig.1 because these TCFs wane long before the onset of slow molecular reorientational processes. Overall, the simulations describe very well the dielectric spectrum of water. The internal vibrations are easily reproduced using a flexible model for water. The absorption at $150\text{-}200 \text{ cm}^{-1}$ was later shown to stem from hindered translational vibrations of the molecule in the cage formed by its neighbors, just as portrayed by the dynamics of the O atoms shown in Fig.1. Indeed, purely translational motions in a system of nonpolarizable molecules such as TIP4P water have only an indirect influence on the fluctuations of the total dipole $M(t)$. When polarizability is taken into account, the translational resonance is well reproduced[23].

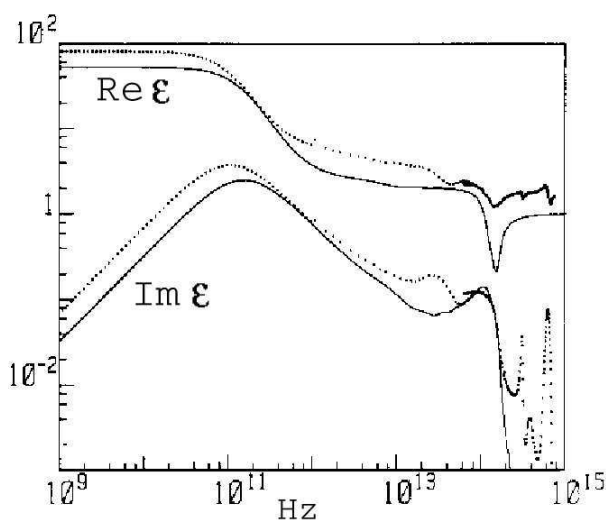


Figure 2. Real and imaginary parts of the frequency dependent dielectric permittivity of water obtained from MD simulations on the TIP4P model (solid lines; Ref.[21]) and experimental data obtained for different regions of the spectrum (dotted lines; Refs.[6, 7])

3.1 Water in DMSO

Dimethylsulfoxide (DMSO) is a highly polar ($\mu \approx 4.3D$) aprotic solvent which mixes with water in all proportions at ambient conditions. The DMSO molecule has an exposed sulfonyl oxygen which acts as a strong hydrogen bond acceptor. For more than forty years, a keen interest has grown over this substance because of its many practical applications in biomedical sciences, industry, and as a medium for chemical reactions[24]. Upon mixing, water and DMSO exhibit interesting changes in thermodynamical, structural, dynamical, and H-bond network properties. In particular, these mixtures present very large deviations from ideal mixing behavior near the composition 33% DMSO, which has been attributed to the formation of strong H-bond aggregates composed of one DMSO and two water molecules (1DMSO:2water). These changes and their molecular origin have been the subject of several MD simulation studies[25]. Analyses of the structure and hydrogen (H)-bond distributions reveal different types of molecular associations, with the prevalence of 1DMSO:2water H-bond aggregates of nearly tetrahedral ordering for water-rich mixtures and 2DMSO:1water linkages for DMSO-rich solutions[26]. The translational and reorientational dynamics of these mixtures investigated through MD simulations are in good agreement with experimental NMR data[27], showing minima for the self-diffusion coefficients and slowest reorientational dynamics for mixtures with composition near 33% DMSO. Simulation studies of the dielectric relaxation[28] over the whole composition range yield results consistent with available measurements[29] and unveils important microscopic details about the behavior of these mixtures.

One of the most interesting MD results on DMSO/water mixtures is the prediction of stable aggregates of composition 2DMSO:1water in DMSO-rich mixtures[26]. While the existence of 1DMSO:2water aggregates seems self-evident in view of the mixing behavior exhibited by several physicochemical properties, unambiguous experimental evidence for the 2DMSO:1water aggregate found in the simulations is still lacking. One of the most conspicuous characteristic of the 2DMSO:1water molecular aggregate is that the central water molecule is flanked by two massive DMSO molecules which strongly interact with it through H-bonding. This “bound” water molecule, being situated in a DMSO-rich microenvironment, is expected to present very different short-time, librational dynamics than that found in pure water. Indeed, our simulations[26, 28] of the far-infrared absorption coefficient for the pure liquids and for mixtures of different compositions predicts an “splitting” of water’s librational band ($600\text{-}800 \text{ cm}^{-1}$) for DMSO-rich mixtures, as shown in Fig. 3. The $F(\omega)$ spectra are approximately given by $\omega \text{Im } \epsilon(\omega)$ for each system and can be directly obtained from experimental far-infrared spectroscopy.

Additional MD analysis permitted a clear identification of the molecular origin for the splitting of water librational band in the presence of DMSO. The calculated spectral characteristics of the TCFs for the angular velocity components for pure water and a mixture with 80% DMSO is shown

in Fig.4 (a schematic drawing of the 2DMSO:1water aggregate is presented on top). The spectrum for pure water consists of the overlap of the individual spectra for each principal component, was mentioned before. In a DMSO-rich environment the spectrum for the angular velocity deconvolutes into two submaxima due to the narrowing of each contribution. The peak in the spectrum for Γ_x shifts from about 850 in pure water to 750 cm^{-1} in the 80% DMSO mixture, indicating that the rapid small-amplitude rotations of the water molecule about the x axis is less hindered in the mixture. This has been rationalized in terms of the aggregate drawn in Fig.4, in which the H-bonding donor character of the water molecule is similar to that in pure water, whereas its acceptor character is very distinct. With practically no H-bonding to its oxygen atom in these environments, the water molecules experience very little restoring forces off the plane of the sheet, thus rendering librations about the x axis less hindered[28].

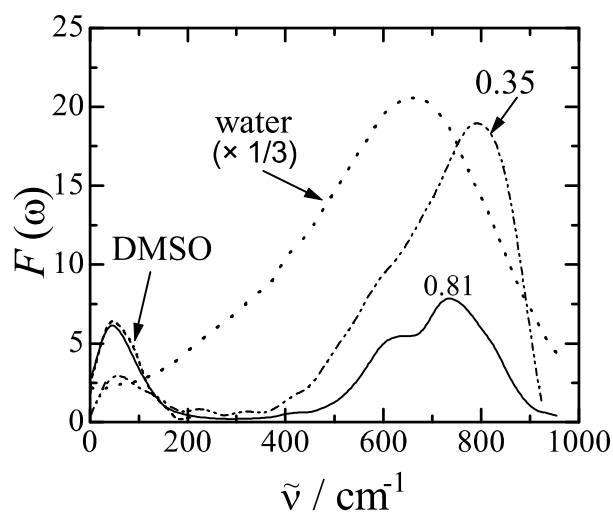


Figure 3. Simulated far-IR spectra for pure DMSO, pure water and two selected DMSO/water mixtures, indicated by the mole fraction of DMSO. The spectrum for pure water has been divided by 3 to fit the scale of the figure.

3.2 Supercritical water

Supercritical states of water provide environments with special properties where many reactive process with important technological applications take place[30]. To give just one example, water under supercritical conditions ($T > T_c = 647\text{K}$) is an extremely powerful, and environmentally benign, oxidizing agent with important applications in the treatment of industrial toxic wastes. Two key aspects combine to make chemical reactivity under these conditions so peculiar: The solvent high compressibility, which allows for large density variations with relatively minor changes in the applied pressure, and the drastic reduction of bulk polarity, clearly manifested in the drop of the macroscopic dielectric constant from $\epsilon \approx 80$ at room temperature to $\epsilon \approx 6$ at near-critical conditions. From a microscopic perspective, the unique features of supercritical fluids as reaction media

are associated with density inhomogeneities present in these systems[31].

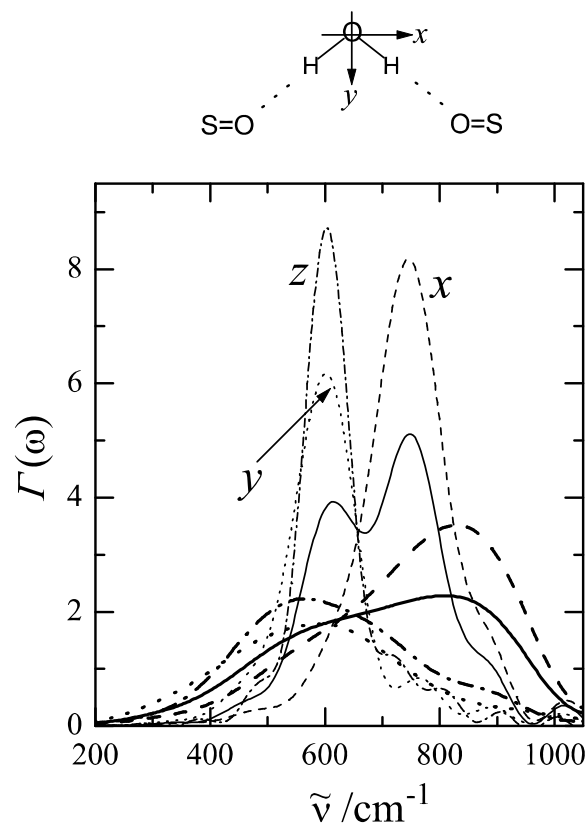


Figure 4. Frequency spectra for the normalized time correlation functions for the principal components of the water molecules' angular velocity in pure water (thick lines) and in an aqueous mixtures with 81% DMSO (thin lines). The drawing is a schematic of the 2DMSO:1water H-bonded aggregate predicted by MD.

Recently, microwave spectroscopy measurements have been reported for SCW at several different densities ranging from $\rho = 1$ down to 0.1 g/cm^3 , in an attempt to provide valuable characterization of the dynamical nature of such reaction media[32]. By fitting the measured frequency-dependent dielectric permittivity with a single Debye dispersion relation, Okada *et al.*[32] have found that the dielectric relaxation time τ_D presents a non-monotonic density dependence, with an unexpected branch for $\rho < 0.4 \text{ g/cm}^3$, showing a rapid increase of τ_D with decreasing density. This interesting feature could lead to distinctive dynamical solvent effects on molecular or ionic probes in solution. This results is surprising because one expects faster, not slower, dipole reorientation as the intermolecular interactions get weaker with decreasing bulk density. In order to investigate the molecular origin of this intriguing effect, we carried out a series of MD simulations for several supercritical thermodynamic states of water with densities ranging from 0.05 up to 1.0 g/cm^3 [33]. Not so much to our surprise, the dielectric relaxation time as function of density for temperatures above T_c (Fig.5) agrees very well with the experimental data for $\rho > 0.4 \text{ g/cm}^3$, but fails to reproduce the rise in τ_D as the

density decreases below this value. The origin of such discrepancy is still not entirely clear, but our analysis indicate that the behavior of the dielectric relaxation time is consistent with the theoretical free-rotor limit as $\rho \rightarrow 0$. The MD analyses[33] also show that the dielectric response is highly nonexponential in the low density regime, which then indicates that the experimental estimates for τ_D obtained from a single Debye fit to the spectra may be highly uncertain. Interestingly, another simulation work, using a much more sophisticated, polarizable water model, was latter published corroborating our results[34]. We believe that further investigations in this area are surely needed.

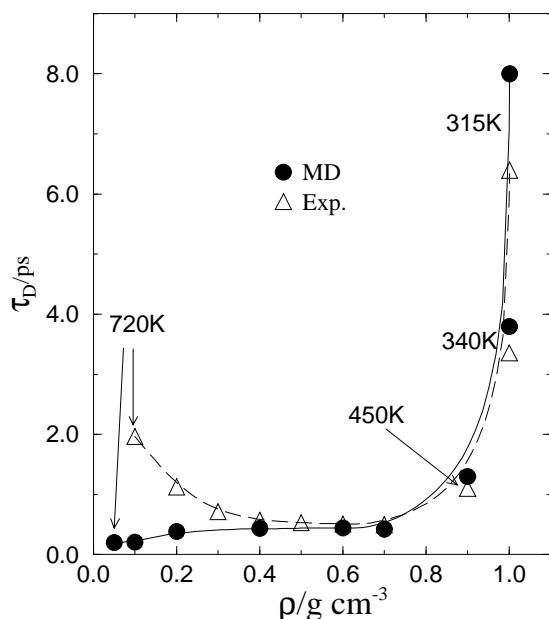


Figure 5. MD and experimental Debye dielectric relaxation times for supercritical water as functions of density. When not indicated, the temperature is 650 K. The lines are drawn as guides to the eye.

4 Time resolved fluorescence

Considerable experimental and theoretical efforts have been devoted to the study of molecular mechanisms of solvation dynamics, that is, the relaxation of the surrounding solvent molecules in response to sudden changes in the spectroscopic solute probe's charge distribution, which are usually brought about a photoinduced transfer of electronic charges from one side of the probe molecule to the other[35, 36]. The study of solvation dynamics at a molecular level comprises an important step towards obtaining a deeper understanding of the dynamical effects of the solvent environment on electron and other charge transfer reactions in solution, and in broader sense of the effects of solvent dynamics on chemical reactions.

Time-dependent Stokes shift spectroscopy provides one means to experimentally access the dynamics of solvation, specially for macroscopically homogeneous environments[35, 36]. In these experiments, the data are usually reported in terms of normalized spectral response

functions describing the temporal evolution of $S(t) = [\nu(t) - \nu(\infty)]/[\nu(0) - \nu(\infty)]$, where $\nu(t)$ refers to the maximum of the emission band at time t . In MD simulations, the photoexcitation is treated within the Frank-Condon approximation, in which the solute's ground and excited states usually differ only by their charge distributions. The corresponding solvation response function is given by

$$S(t) = \frac{\langle \Delta E(t) - \Delta E(\infty) \rangle_{ne}}{\langle \Delta E(0) - \Delta E(\infty) \rangle_{ne}} \quad (2)$$

where $\Delta E(t) = U_{el}^{S_1}(t) - U_{el}^{S_0}(t)$ is the difference between the S_1 and the S_0 Born-Oppenheimer potential energy surfaces and $\langle \dots \rangle_{ne}$ denotes an average taken over the nonequilibrium trajectories. This requires knowledge of the excited and ground state charge distributions of the solute probe, which is usually obtained from quantum chemical electronic structure calculations. The family of organic dyes known as coumarins are among the most popular chromophores used to investigate solvation dynamics in liquids. Coumarin 153 (C153) is one of them.

4.1 Binary aqueous mixtures

Our studies on the solvation dynamics of aqueous systems have focused on binary mixtures of water-methanol[37] and more recently on water-DMSO mixtures. For the latter, we have performed studies using a simplified monoatomic model for the solute[38] in which we were able to identify important contributions from water translational motions to the solvation dynamics, manifested as a surprising negative branch on the individual co-solvent contributions to the total solvation response. Our MD studies on solvation dynamics of water-DMSO systems have been extended towards a more realistic description of the organic dyes[39] using a more elaborate all-atom model for the coumarin C153 in which we sought direct comparison with very recent experimental upconversion fluorescence spectroscopy measurements. Nonequilibrium simulation results for the solvation response $S(t)$ of C153 in the neat liquids and various water-DMSO mixtures are shown in Fig.6a. One can see that the solvation dynamics of the aqueous systems exhibit an ultrafast initial relaxation within tens of femtoseconds, which becomes less prominent as DMSO is added to the system. The fast oscillations exhibited by the $S(t)$ responses stem from the fast librational motions of water molecules. The post-librational regime is characterized by a bi-exponential decay stemming from rotational-diffusion processes with some translational contributions. In all cases, the solvation dynamics is completed almost entirely on a subpicosecond time scale. The relaxation is most sluggish for mixtures of composition near 25% DMSO, in accordance with previous simulations and experimental results on diffusional processes of these mixtures. Our MD results show excellent agreement with time resolved experimental data (Fig.6b)[40] after taking into account the finite resolution of the experimental setup through a convolution of the MD data with an instrument response function.

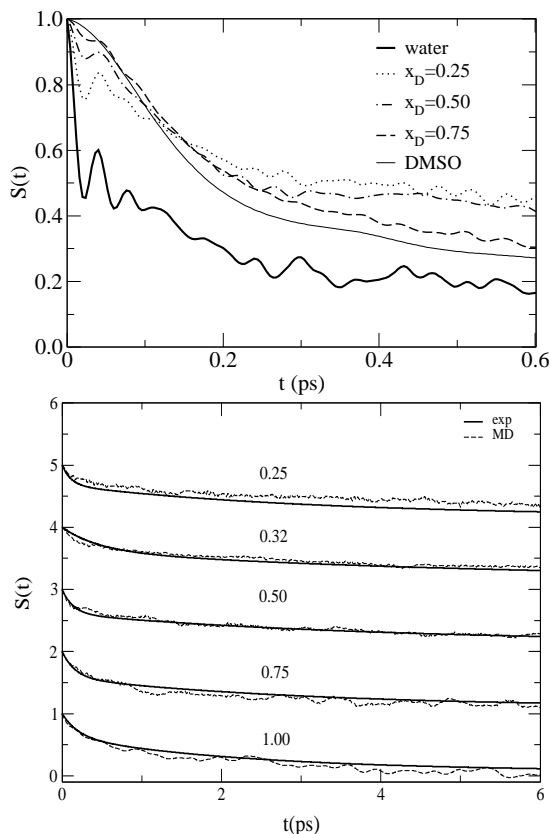


Figure 6. Nonequilibrium solvation responses for pure water and DMSO and selected DMSO/water mixtures obtained from MD simulations using an all-atom model for the coumarin C153.

4.2 Hydrated electrons

The hydrated electron (an excess electron trapped into the solvent) is an excellent probe for time-dependent spectroscopies because of its large optical cross-section and the sufficiently long lifetime of the first excited state[41]. From the theoretical viewpoint, the solvated electron is also the prototype system for mixed quantum-classical (MQC) simulations and has been extensively used in the development of new computational methodologies and the exploration of a variety of new physical phenomena in condensed media[42]. In such MQC simulations the dynamics of the quantum particle (the electron) is fully described within the bath of classical solvent molecules. Previous simulation studies of the nonadiabatic relaxation from excited states[43] and the dynamics of solvent reorganization in response to the photoexcitation of a self-trapped electron in aqueous solution[44] have revealed that the dynamical behavior of this system is extremely rich. In summary, the solvation dynamics response resembles that of classical solutes in polar liquids, with an initial Gaussian decay characterized by a ~ 17 fs decay time, followed by a slower (250 fs) exponential decay comprising roughly 60% of the relaxation. However, unlike most classical perturbations, the solvation mechanisms involve considerable solvent translational motions in order to accommodate the changes in shape and size of the electronic wavefunction upon photoexcitation (from an s -like ground

state to a p -like first excited state) or after a nonadiabatic transition (from p - to s -like states). The relative importance of fast solvent librations in comparison with translational motions to the different stages of solvation process was not entirely clear for the hydrated electron.

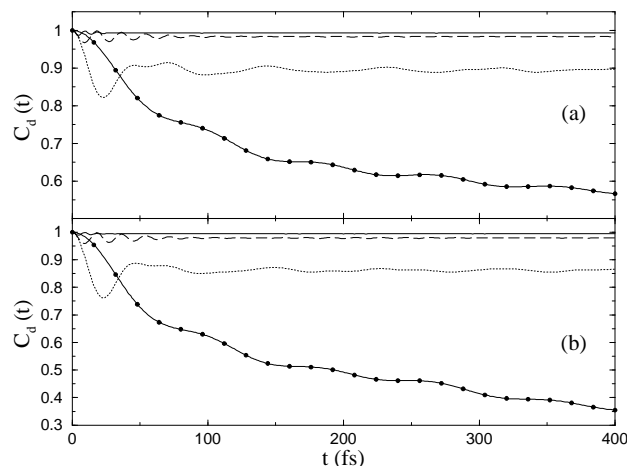


Figure 7. Comparison between simulation and experimental solvation responses for C153 in DMSO/water mixtures (thick lines) after convolution of the MD response with a Gaussian function representing the instrument time resolution. The Gaussian is centered at 200 fs for pure DMSO and the $x_D = 0.75$ solution, and at 140 fs for the other mixtures.

Very important and extensive theoretical work on solvated electrons have been carried by the Rossky group. Further understanding of the dynamical behavior of hydrated electrons has been reached by applying the instantaneous normal mode (INM) theoretical framework of liquids to MQC simulations[45]. From the very extensive analysis of that work, we will discuss here only the relative contributions from the different types of solvent motions to the electron solvation response that we extracted from the INM formalism. Consistently with a variety of spectroscopic measurements on liquid water, we have separated the motions within INM according to the frequency ranges: Diffusive: $0 - 400$ cm^{-1} ; Librational: $400 - 1200$ cm^{-1} ; Bending: $1500 - 2200$ cm^{-1} ; and Stretching: $2200 - 4600$ cm^{-1} . Fig. 7 shows the normalized partial solvation responses from the four frequency ranges for the upward (panel a) and downward (panel b) electronic transitions. The partial responses exhibit similar features for both cases. The internal bending and stretching motions are seen to contribute to the solvation responses only at very early times, typically below 5-10 fs, which may possibly impact quantum decoherence of the electronic states. The fast librational motions dominate most of the response in the first 25 fs and is also the cause of the recurrence in the total response functions at ~ 40 fs. Diffusive motions also come in at early stages of the solvation process, being the predominant relaxation channel from about 50 fs and on. This result indicates the importance of translational dynamics to the solvation response in these systems and shows that the combination of librational and diffusive motions comes in at an early stages of the solvation

response of the hydrated electron. Moreover, the characteristics of the diffusive contributions are distinct from those of the librational and single-molecule internal modes. In the phenomenological Brownian oscillator picture, the former behaves like an overdamped oscillator, whereas the behavior of the librations and intramolecular vibrations is typically underdamped. From the viewpoint of the INM theory, these features stem from the different degrees of localization of the diffusive, librational, and internal motions. Further comparison of panels (a) and (b) of Fig.7 suggests that both librational and diffusive contributions are slightly larger for the downward than for the upward transition. This difference is clearly associated with the spatial shrinkage of the electron wavefunction for the downward transition which creates a void readily occupied by the neighboring solvent molecules, starting with the rapid dragging in of the light hydrogen atoms.

4.3 Electrons in supercritical water

Another interesting problem where mixed quantum-classical simulations contributed with new physical insights is that of the quantum states of excess electrons solvated in supercritical fluids. In normal dense fluids, the ground and first few excited state wavefunctions for the solvated electron are spatially localized in a roughly spherical region not much larger than a halogen anion due to the interactions with the surrounding solvent molecules. In a hypothetical situation in which the number density of the solvent environment is gradually reduced down to nearly zero, one would expect the excess electron wavefunction to change from a spatially localized to a delocalized, quasifree state over the entire volume near $\rho = 0$, resembling the text-book problem of a particle in a box. With supercritical fluids, this situation can in principle be materialized since the density can be drastically varied by small variations of the external pressure[31].

For many years, a series of pulse radiolysis experiments has provided evidence that electronic states can be supported in aqueous supercritical environments[46, 47, 48] and that the spectral characteristics of solvated electrons can be used to investigate the structure of the local inhomogeneities in supercritical systems[49]. It is generally believed that a gradual transition from localized states, typical of dense polar fluids, to quasifree electronic states under supercritical conditions leads to the observed red shifts in the optical absorption spectra and to significant changes in the dynamical behavior of the electron, most notably a dramatic increase in its drift mobility[50]. However, experimental[46] absorption spectra of nearly supercritical water at $T = 623$ K exhibit a weak density dependence of the spectral shift over a wide interval ranging from 1 g cm^{-3} down to 0.05 g cm^{-3} , thus suggesting that the electron localization in aqueous supercritical environments persists at density as low as 0.05 g cm^{-3} .

Laria and Skaf[51] recently addressed this problem by simulating an excess quantum electron in a bath of classical water using Feynman Path Integral MD techniques. This formalism explores the well-known isomorphism between the statistical mechanics of the quantum electron path and

that of a classical cyclic polymer containing pseudoparticles (“beads”) with harmonic nearest neighbor interactions. The most direct route to analyze the extent of the electronic localization is by examining the behavior of the mean square correlation function for the solvated electron-polymer $\mathcal{R}^2(t)$ defined by:

$$\mathcal{R}^2(t - t') = \langle |\mathbf{r}(t) - \mathbf{r}(t')|^2 \rangle, \quad 0 \leq t - t' \leq \beta\hbar; \quad (3)$$

where $\mathbf{r}(t)$ represents the electron position at imaginary time t and β^{-1} is Boltzmann constant times the temperature. At low densities ($\rho_w < 0.1 \text{ g cm}^{-3}$), the correlation functions (Fig. 8, left panel) look similar to those corresponding to Gaussian free polymers: Interparticle distances along the electron polymer are characterized by a wide variety of lengthscales, up to roughly half the de Broglie thermal wavelength, $\lambda_{dB}(T = 645 \text{ K}) \approx 12 \text{ \AA}$. As we move towards the density regime of typical dense fluids, there is a qualitative change in the temporal behavior of the curves. After a short transient lasting $\approx 0.1\beta\hbar$, the curves level off at practically plateau values. This time independence has been interpreted as a signature of statistical dominance of the ground state on the behavior of the electron. Expressed in terms of the spectrum of instantaneous electron eigenvalues, this situation corresponds to large energy gaps ($\gg k_B T$) between the ground and the manifold of excited states. More direct evidence of this transition is acquired by inspecting the density dependence of the correlation length for the electron polymer $\mathcal{R} = \mathcal{R}(\beta\hbar/2)$, shown in the right panel of Fig.8. The sudden drop to practically half of the ideal, non-interacting, $\rho_w = 0$ value within a narrow density interval and an abrupt change in the slope of the curve, reveal the onset of the electronic localization at $\rho_w \approx 0.15 \text{ g cm}^{-3}$. For densities well below the localization threshold, one can see the electron wavefunction tunneling across the surrounding water molecules.

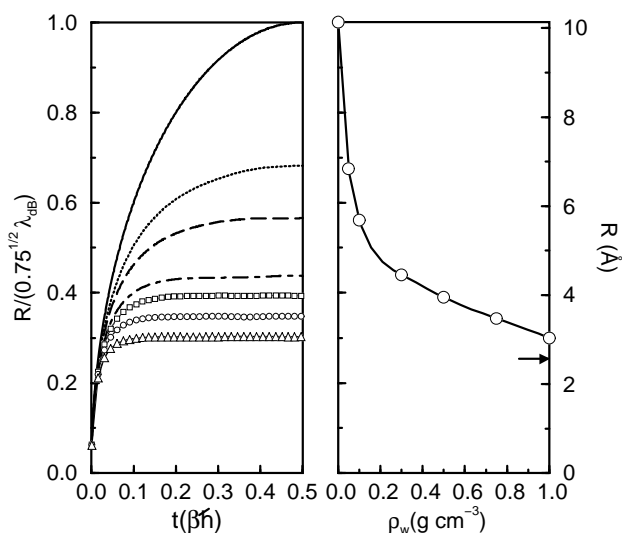


Figure 8. Left: Root mean square correlation function for the excess electron in supercritical water along the $T = 645$ K isotherm. Lines from top to bottom correspond to $\rho_w = 0.0$ (free electron), 0.05, 0.1, 0.3, 0.5, 0.7, and 1.0 g cm^{-3} , respectively. Right: Correlation length for the electron polymer vs. density. The arrow indicates the room temperature result.

The optical absorption spectra for supercritical states of water were also computed from our simulations and they reproduce the experimental values reasonably well, although the density dependence of the spectral red shift in the range $0.1 \text{ g cm}^{-3} \leq \rho_w \leq 0.5 \text{ g cm}^{-3}$ is somewhat more pronounced than that experimentally measured. Interestingly, there are apparently no noticeable changes in the density dependence of the spectral band maximum as the localization transition is crossed.

5 Ultrafast optical Kerr effect

The optical Kerr effect (OKE) ultrafast laser spectroscopy is part of a large family of multiple-wave mixing processes that exploits nonlinear optical responses of the material to extract information on its ultrarapid intra- and intermolecular dynamics directly in time domain[14]. OKE spectroscopy has been successfully applied to extract dynamical information of a large variety of pure liquids, mixtures, and confined fluids[52]. In liquid water, the nonlinear optical signal is dominated by the electronic polarizability response, as the motion of the nuclei provides less than 5% of the total response. This increases the degree of uncertainty in obtaining the dynamics of water and here is where MD simulations come in.

The optically heterodyne-detected OKE signal in the time domain reflects the third order electric susceptibility of the sample and provides valuable information about the intermolecular dynamics through the nuclear response function, $R^{\text{nuc}}(t)$. This quantity is experimentally obtained from the raw OKE transients after removal of the instantaneous electronic response and deconvolution from the instrument function[53]. $R^{\text{nuc}}(t)$ can also be fairly easily obtained from a sufficiently long set of MD trajectories by simply computing the time derivative of the anisotropy collective polarizability TCF through:

$$R^{\text{nuc}}(t) = -\frac{\Theta(t)}{k_B T} \frac{\partial \Psi(t)}{\partial t}, \quad (4)$$

where $\Theta(t)$ is the Heaviside step function and $\Psi(t) \propto \langle \Pi_{xz}(t) \Pi_{xz}(0) \rangle$ is the TCF of the polarizability anisotropy, with

$$\Pi = \sum_i \alpha_i = \Pi^M + \Pi^I, \quad (5)$$

where the total polarizability has been separated into intrinsic (molecular), Π^M , and induced, Π^I contributions. The intrinsic part is the sum of unperturbed, gas phase molecular polarizabilities properly rotated into the lab frame of reference, while the induced counterpart is computed through some induction or modulation scheme such as the dipole-induced-dipole mechanism.

We have studied the OKE response for pure water and also in water-DMSO mixtures using molecular polarizability and hyperpolarizability tensors obtained from electronic structure calculations at the MP2/6-311++G(d,p) level in our MD simulation analysis[54]. The results for $R^{\text{nuc}}(t)$

of liquid water are shown in Fig.9, along with the permanent or molecular polarizability autocorrelation, induced polarizability contributions and the cross-correlation between permanent and induced anisotropies. The simulated OKE nuclear response exhibits a very rapid rise within the initial stages, showing local maxima near 15, 50, and 180 fs, followed by a diffusive tail which has been fitted by a bi-exponential with time constants ~ 0.2 and 2.0 ps. The short time features are in good agreement with previous simulations as well as with experimental results reported by Castner *et al.*[55], which shows peaks at ~ 20 , 57, and 197 fs. The agreement with experiments is less satisfactory for the diffusive components. Figure 9 also shows that the first peak is almost entirely given by fast molecular reorientational that clearly associated to librational motions, while the subsequent maxima stem from a combination of permanent and induced contributions. The maximum near 180 fs seems to have important contributions from translational dynamics as indicated by the amplitude of the induced term around that time window. The hindered translational motions of the O atoms comprise the underlying molecular mechanism for this feature.

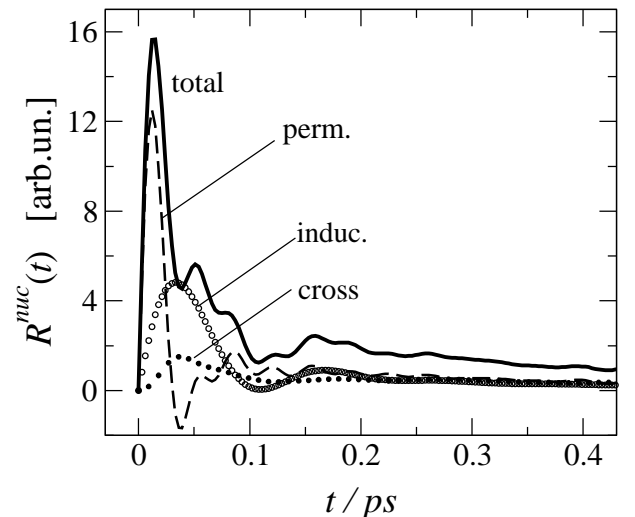


Figure 9. The OKE nuclear response function for water obtained from MD simulations. The total response and the separate contributions are as indicated.

These response functions can be appropriately Fourier transformed to represent either the frequency spectrum of the Kerr signal or the Bose-Einstein corrected depolarized Raman spectrum. Although we do not show these spectra here, it is important to mention that the simulated OKE spectrum for water exhibits a rotational-diffusion peak centered around 3 cm^{-1} , a collision-induced (hindered translations) band near 200 cm^{-1} , and a broad librational band at 450 cm^{-1} . These results are in good agreement with experimental frequency spectra obtained from Kerr effect and related spectroscopies. There are, however, noticeable discrepancies in the vicinity of 60 cm^{-1} , indicating shortcomings in our modeling of the polarizability fluctuations of water.

6 Vibrational Dephasing

Vibrational dephasing refers to the lost of coherence by a collection of oscillators coupled to a solvent bath[56]. Imagine an oscillator whose vibrational motion is being perturbed by the fluctuating interactions with the surrounding solvent. The phase of the oscillations will soon go random due to the fluctuations in the intermolecular potential. In this phenomenon, both the timescale and magnitude of the force fluctuations are important[57]. Valuable information about the solvent dynamics can be extracted from a vibrational dephasing analysis of Raman lineshapes if a sensitive Raman probe is used. In recent years, vibrational dephasing have also been investigated directly in the time domain using ultrafast laser spectroscopies such as Raman echo or Raman free-induction decay[13].

The monocyclic dianions, $C_nO_n^{2-}$ ($3 \leq n \leq 6$), known as oxocarbon dianions comprise a family of excellent Raman probes[58]. The squarate ($n = 4$) and croconate ($n = 5$) ions exhibit unusually high Raman intensities for both totally symmetric and non-totally symmetric modes, with relatively well-separated bands. Such a distinctive property has been used to examine the Raman lineshapes of modes of different symmetries in aqueous solutions, thus providing an experimental route the reorientational dynamics about the in-plane and out-of-plane symmetry axes of the oxocarbons[58]. Detailed analyses based on the isotropic and anisotropic components of the totally symmetric ring breathing mode, along with the anisotropic parts of the non-totally symmetric C-C stretching and ring bending modes, indicate that reorientation of the oxocarbon anions is very hindered in water, with comparable decay rates for spinning and tumbling of the main symmetry axis. Vibrational dephasing analysis predicted small relaxation times (~ 0.1 ps) of the vibrational frequency fluctuations. This fast modulation together with the observed slow rotational-diffusion dynamics suggests a picture where the ions undergo rapid librational motions inside solvent cages, which are continually formed and disrupted on a timescale that should exceed several times the characteristic librational period.

Indeed, our recent MD simulation studies of the squarate in water show the existence of a well-defined hydration shell, composed of an average of 12 water molecules H-bonded to the carbonyl oxygens (three water molecules per oxygen atom) which is preserved for more than 20-30 ps[59, 60]. The dynamics is isotropic and the anion librates at 70 and 250 cm^{-1} [60]. In a separate MD study, we have also investigated more closely the features of the vibrational dephasing of this species in water. Within the classical theory of vibrational dephasing, the instantaneous shift in the vibration frequency of mode α is related to solvent resultant forces along the coordinates of the normal mode of interest during the simulations, the anharmonicity constants, $\phi_{\alpha\beta\gamma}$, and the atomic displacements of each mode, L_m^α , which are obtained from a quantum chemical vibrational analysis of the isolated molecule[56]:

$$\delta\omega^\alpha(t) = \sum_{\beta}^{\text{modes}} \phi_{\alpha\alpha\beta} \sum_m^{\text{soluteatoms}} L_m^\beta F_m(t) \quad (6)$$

The quantity of interest is the frequency shift dynamical fluctuations:

$$\chi^\alpha(t) = \langle \Delta\omega^\alpha(t)\Delta\omega^\alpha(0) \rangle ; \quad \Delta\omega^\alpha(t) = \delta\omega^\alpha(t) - \langle \delta\omega^\alpha \rangle \quad (7)$$

from which one can compute the dephasing time $1/T_2^\alpha = \int_0^\infty \chi^\alpha(t)dt$ for direct comparison with experimental measurements.

Out of all normal modes of the squarate dianion, the C=O stretching (ν_1) and ring breathing (ν_2) modes are particularly interesting because their use in the experimental analysis. The ring breathing dephasing time obtained from the simulations (0.08 ps) is in close agreement with the experimental estimates (0.06 ps). The frequency shift correlation function separated in terms of the purely Coulombic, $\chi_C(t)$, and short-ranged dispersive (Lennard-Jones) forces, $\chi_{LJ}(t)$, for these two vibrational modes are shown in Fig.10. The results show that the electrostatic forces contributions to the dephasing exhibit fast dynamics at early times, clearly associated to the rapid motions of water hydrogen atoms, that is, solvent librations, but also present a slower component at longer times due to long-range nature of the Coulombic interactions. The dispersive contributions, on the other hand, fluctuates with larger timescales because it involves motions of the oxygen atoms (the hydrogens have vanishing dispersive interactions), but show no long-time tail since $\chi_{LJ}(t)$ is essentially determined by the short-range structure of the liquid. Fig. 10 also shows the dephasing responses for each mode with (thin lines) and without (thick lines) the anharmonic couplings between modes (cf. Eq.6). One sees that mode coupling affects essentially the LJ part of the dephasing correlation function for the C=O stretching, leaving the other correlations practically unaltered.

7 Water near interfaces

The heterogeneous nature of interfacial liquid/liquid systems have long been a subject of keen interest to scientists and motivated widespread studies about microphysical behavior at interfaces. At molecular scales, the system's broken symmetry imposes a nonconventional ambient in the immediate vicinity of the interface, resulting in a molecular behavior that can be much different from that found in the bulk liquid phase. Liquid interfaces also play an important role in biological systems, such as membranes and proteins outer surfaces, and in colloid sciences, which very often involve systems of great practical and technological importance. In recent years, new approaches based on nonlinear spectroscopic methods have provided important insights and detailed information about the structural and dynamical behavior of molecules at interfaces[61, 62]. While a great deal of our current knowledge on interfacial systems has been obtained from measurements of thermodynamic macroscopic properties, nonlinear spectroscopic techniques such as Second Harmonic Generation (SHG) and Vibrational Sum Frequency (VSF), have made it possible to investigate the behavior of molecules located in the vicinity of the interface without the interfering signal from molecules situated in the bulk[61, 62].

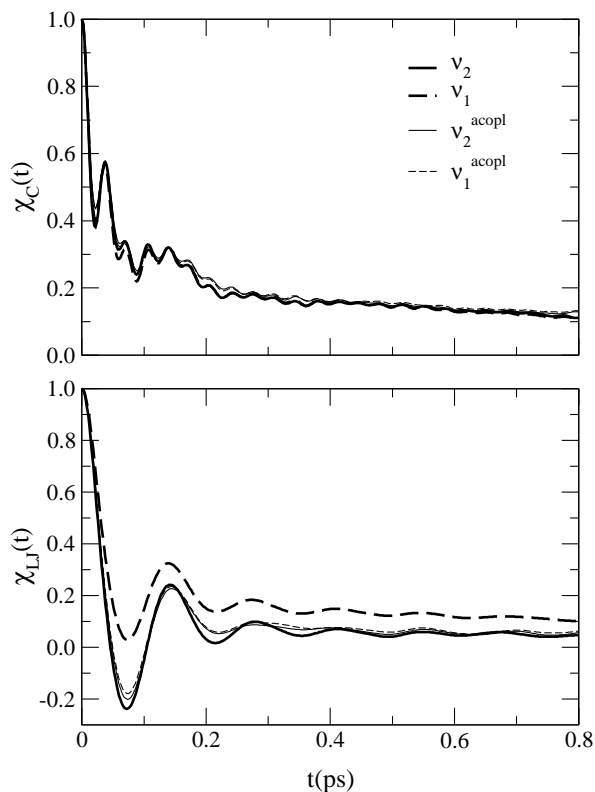


Figure 10. Dephasing responses obtained for the C=O stretching (ν_1 and ring breathing (ν_2) modes of the squarate anion in water. The upper and lower panel depicts the Coulombic and dispersive contributions, respectively.

Of particular interest, the water/carbon tetrachloride ($\text{H}_2\text{O}/\text{CCl}_4$) interface emerges as an important prototype for hydrophobic interacting systems that grossly mimic biological membranes, and as a natural support media for surfactant systems in molecular simulation studies. In addition, the CCl_4 molecules are quite insensitive to infrared radiation absorption, eliminating possible interferences in non-linear spectroscopy of interfacial water molecules. Very recently, we have performed extensive MD simulations for the $\text{H}_2\text{O}/\text{CCl}_4$ liquid/liquid interface aiming at elucidating the general structural and dynamical features of this interface at a microscopic level[63]. We present next MD results regarding the orientation of water molecules near the interface and how it influences the dynamics of interfacial water. The simulations were performed using models that include internal vibrations.

The average orientation of the water molecules with respect to the plane of the interface is an important structural feature that can be determined from the normalized probability distribution for the angle between the water dipole and the Z axis (normal to the interface), and also for the angle between the Z axis and the vector joining the hydrogen atoms of a given molecule. For clarity, we denote μ_z and HH_z the Z components of the unitary dipole and HH vectors, respectively. The results are depicted in Fig.11a and 11b for bulk (dashed lines) and interfacial (solid lines) water molecules. For comparison, Fig.11a also shows the distribution of the dipoles' Z components for an intermediate region between

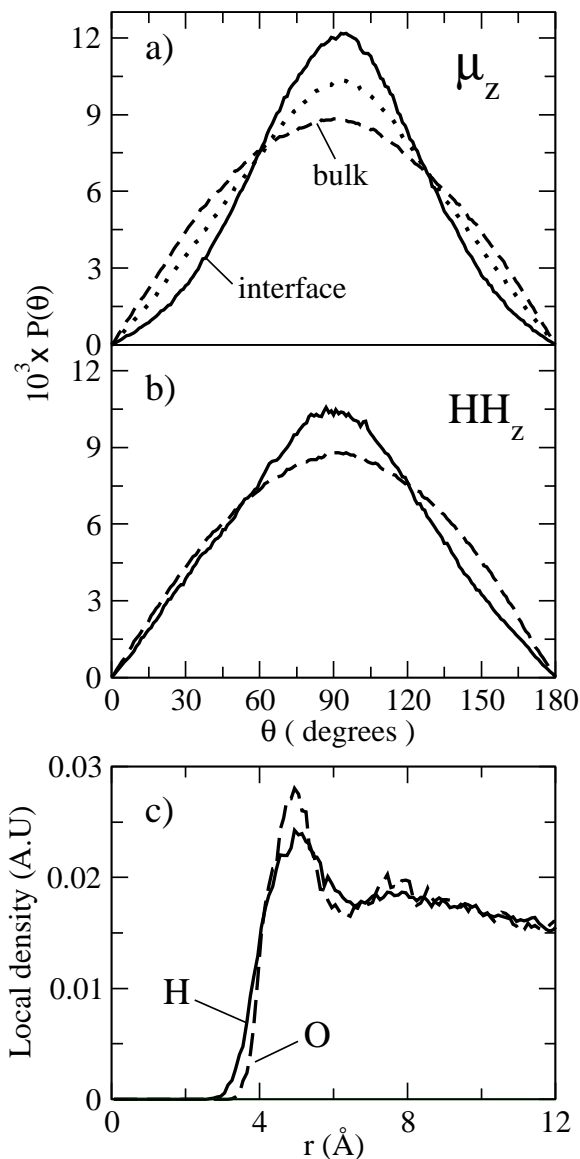


Figure 11. Probability distributions for the angle between the Z axis (normal to interface) and the unit dipole (panel a) and HH vectors (panel b) for bulk and interfacial regions obtained from MD simulations of a water/ CCl_4 liquid/liquid interface.

bulk and interface (dotted line). For an isotropic environment such as bulk liquid, the orientation of any molecular vector follows an uniform distribution, which in polar coordinates is simply given by $P^{\text{iso}}(\theta) = 1/2 \sin(\theta)$. Indeed, the bulk distributions shown in Fig.11 are sinusoidal. As one approaches the interface, there is a relative enhancement in the population of water dipoles oriented parallel to the interface with the concomitant decrease in the probability of finding a water molecule with the main symmetry axis pointing across the interface (Fig.11a). A similar behavior is observed for the HH vectors (Fig.11b). However, in this case one notices a slight asymmetry in the distribution which implies that near the interface the HH vectors are, on the average, slightly twisted at angle from the interface plane. Similar conclusions have been reported in previous MD simulations

of this interface, although in less detailed molecular terms. Further support to this observation is provided by the local density of hydrogen and oxygen atoms as measured from the center of masses of CCl_4 molecules located at the interface. Fig. 11c shows the local density for the H (solid line) and O (dashed line) atoms in arbitrary units. The local density of H atoms is divided by two, such that at larger distances it coincides with the local density of O atoms. Fig. 11c clearly shows that in going from the organic to the aqueous phase one would encounter a water hydrogen first. Analysis of the H-bond distribution shows that, near the interface, the average number of H-bonds per water molecule is only 2.7, indicating the presence of “free” OH bonds.

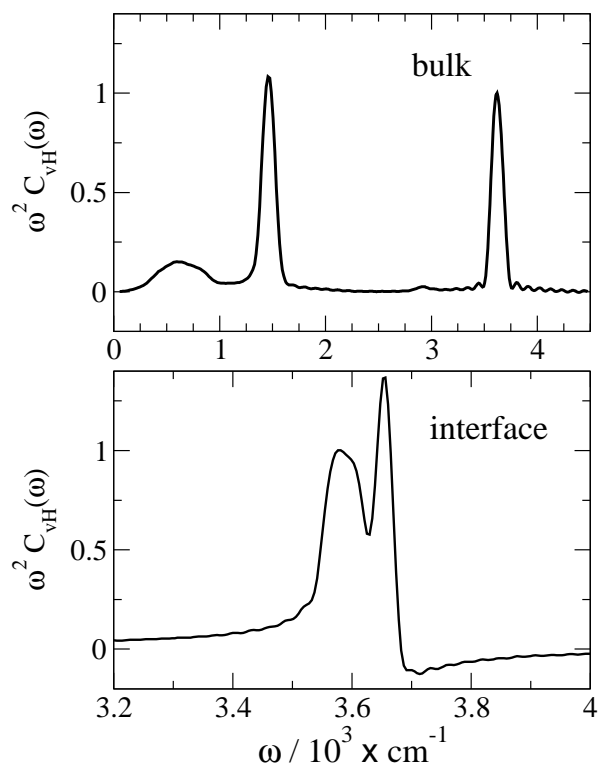


Figure 12. Frequency spectra for the water hydrogen atoms velocity time correlation for molecules in the bulk phase (upper panel) obtained from MD simulations. The lower band ($< 1000 \text{ cm}^{-1}$) is due to intermolecular librations and the two upper bands reflect the bond bending and stretching modes. The lower panel shows the spectrum in the region of stretching modes for water near the CCl_4 interface.

The dynamics of the water molecules in the vicinity of the CCl_4 interface can be investigated in several different ways. One of the simplest and most elucidating form of unveiling this dynamics is through the frequency spectrum of the hydrogen velocity TCF, $C_{vH}(t)$. Fig. 12 shows the $\tilde{C}_{vH}(\omega)$ spectra of the hydrogen dynamics for bulk water molecules. The intermolecular, librational band discussed before that appears below 1000 cm^{-1} is clearly seen for both bulk and interface water. The sharp peaks near 1500 and 3600 cm^{-1} stand for the bond bending and stretching internal modes (symmetric and antisymmetric altogether). The

lower panel shows the spectrum in the region of the stretching modes for water near the interface with CCl_4 . The spectrum is remarkably similar to that obtained experimentally through VSF spectroscopy of this interface[61], thus reinforcing the view that near these interfaces there should exist “free” OH bonds. Further research in this direction is currently being conducted.

8 Ligand-protein dissociation

Water has also a fundamental role on the structure and dynamics of biomolecules, particularly proteins. From the point of view of molecular dynamics simulations, this introduces significant challenges, since the complete solvation of a large biomolecule requires tens of thousands of water molecules, increasing by orders of magnitude the computational demand. Thus, it is common to neglect the effect of water molecules, even without rigorous studies on the role of water in the simulations being performed.

One of the main fields where molecular dynamics simulations is able to provide valuable insights is the association and dissociation pathways of ligands into or from their receptors. Among these receptors a very important class is the Nuclear Hormone Receptor Superfamily, which controls the activity of the most important hormones in vertebrates, such as the Retinoic Acid (Vitamin A), Estrogen and Thyroid hormones, for example. The pathways of dissociation of the Retinoic Acid from its receptor RAR- γ were accessed through molecular dynamics simulations by Karplus and co-workers by a technique known as Enhanced Sampling Molecular Dynamics (ESMD) which is designed, basically, to reduce the potential barriers for ligand escape increasing the dissociation rates [64]. This is achieved by simulating a collection of hormone replicas in the presence of a unique protein in such a way that the replicas do not interact with each other while the interaction with the protein is scaled by the number of hormone replicas being used in the simulation. This permits the simulation of the dissociation pathways in time scales accessible for MD simulations.

The simulations of Karplus and co-workers were performed without any water molecule due to the computational cost of simulating the solvent. This was consistent with the use of a technique where the potential parameters of interactions are approximated with the goal of increasing dissociation rates. They observed a mechanism that was already suggested in the literature [65] known as “mouse trap”, which is represented in Fig.13 and consists basically on the movement of the Helix 12 apart from the body of the protein, forming a cavity through which the hormones escape. They observed this pathway in less than 100 ps, as is shown in Fig.13.

While there would be no great improvement on the significance of the results by the inclusion of the solvent since potentials were already approximated, it is not known whether the water molecules that actually belong to the crystallographic structure would be of any relevance to the dissociation pathway. This problem is particularly important since these water molecules belong to the protein in

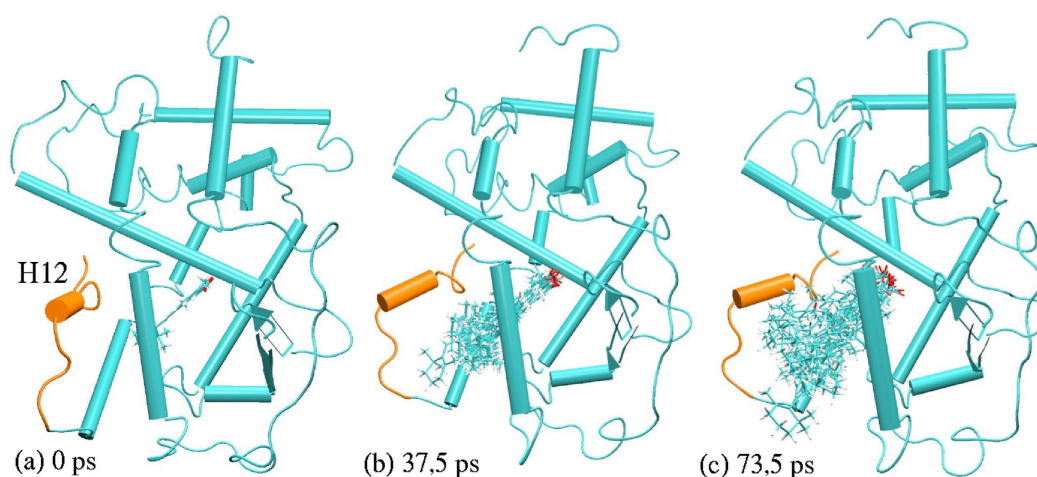


Figure 13. Dissociation pathway of the retinoic acid from its receptor resembling the “mouse trap” mechanism obtained from ESMD simulations in the absence of solvent molecules.

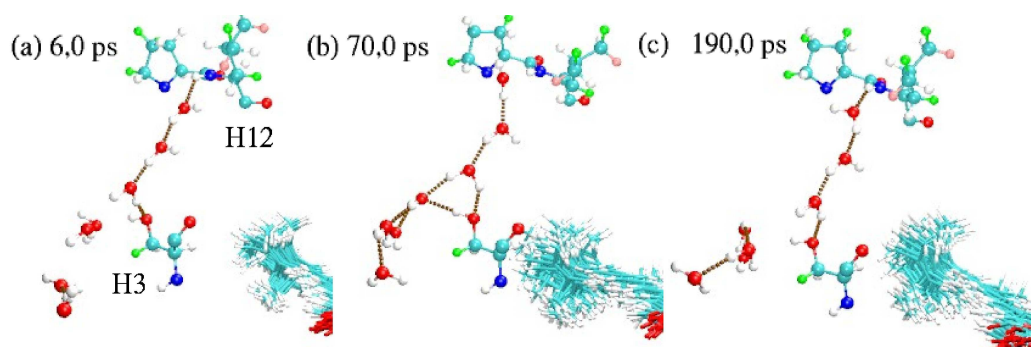


Figure 14. Detail of the dissociation pathway of the retinoic acid from its receptor showing stabilization of the protein structure through a H-bond network promoted by the presence of structural water molecules.

the sense that their residence time in the corresponding positions relative to the protein structure is very long compared water diffusion in bulk solvent [66]. We then performed ESMD simulations with the same protein, hormone and techniques used by Karplus and co-workers to access the role of structural water molecules in the dissociation pathways proposed [67]. We performed four independent simulations with 20 and 50 retinoic acid replicas, with and without the presence of crystallographic water molecules, for 200 ps each. The first simulation reproduced part of the results presented in [64], revealing, indeed, the “mouse trap” mechanism in the same time scale as shown in Fig. 13.

However, the simulation with 20 hormone replicas in the presence of structural water molecules did not lead any hormone dissociation within 200 ps, which is more than twice the time needed to dissociate in the absence of water. The detailed observation of the dynamics of the water molecules in the region where the Helix 12 should lose its interactions to the protein leading to dissociation in the 20 copies simulation unveils important information about the interaction of water with key aminoacids. As shown in Fig. 14, while the Serine in the bottom of the Figure belongs to the protein body, the Proline and Leucine at the top belong to the Helix 12. Clearly, the water molecules form bridges of three or four hydrogen bonded molecules between these aminoacids

throughout the course of the simulation. This restrains the movement of the Helix 12 and, thus, hinders hormone escaping from the receptor’s cavity.

This result has shown that while the structural water molecules did not promote a different pathway for dissociation, they significantly decrease the dissociation rate by stabilizing the protein structure. This is a novel and interesting example of the very important role that water plays to biomolecular structure and dynamics, and that it has an active role on the functionality of protein structures.

9 Concluding Remarks

We have presented a review on the dynamical properties of several aqueous systems focused largely on computer simulation work performed in our lab at the State University of Campinas. With this mosaic, hope to have given the reader, specially the nonexpert in this field, a glimpse at the fascinating dynamical behavior of water.

Acknowledgements

The authors gratefully acknowledge FAPESP and CNPq for supporting most of the work done in our lab. MSS would like to thank Ivana A. Borin for the initial work on water/DMSO mixtures. It is a pleasure to thank Professors

Daniel Laria, Mauro Ribeiro, Branka Ladanyi, Peter Rossky, and Igor Polikarpov for their wonderful collaboration.

References

- [1] F. H. Stillinger, *Adv. Chem. Phys.* **31**, 1 (1975); *Science* **209**, 451 (1980). Over the years, there have been innumerable excellent reviews on water and aqueous systems. These and the next three references serve as a starting point to the literature and reflects the authors personal choice. More recent review articles can be found by a quick bibliographic search over the Internet.
- [2] P. J. Rossky, *Annu. Rev. Phys. Chem.* **36**, 321 (1985).
- [3] B. M. Ladanyi and M. S. Skaf, *Annu. Rev. Phys. Chem.* **44**, 335 (1993).
- [4] I. Ohmine and H. Tanaka, *Chem. Rev.* **7**, 2545 (1993).
- [5] K. Liu, M. G. Brown, C. Carter, R. J. Saykally, and D. C. Clary, *Nature* **381**, 501 (1996); F. N. Keutsch, and R. J. Saykally, *Proc. Nat. Acad. Sci. (USA)* **98**, 10533 (2001).
- [6] U. Kaatze and V. Uhlenndorf, *Z. Phys. Chem. N. F.* **126**, 151 (1981).
- [7] M. N. Afsar and J. B. Hasted, *J. Opt. Soc. Am.* **67**, 902 (1977); J. B. Hasted, S. K. Husain, F. A. M. Frescura, and J. R. Birch, *Chem. Phys. Lett.* **118**, 622 (1985); A. N. Rusk, D. Williams, and M. R. Querry, *J. Opt. Soc. Am.* **61**, 895 (1971).
- [8] A. de Santis, M. Sampoli, V. Mazzacurati, and M. A. Ricci, *Chem. Phys. Lett.* **133**, 381 (1987); A. de Santis, R. Frattini, M. Sampoli, V. Mazzacurati, M. Nardone, M. A. Ricci, and G. Ruocco, *Mol. Phys.* **61**, 1199 (1987).
- [9] C. J. Montrose, J. A. Bucaro, J. Marshall-Coakley, and T. A. Litowitz, *J. Chem. Phys.* **60**, 5025 (1974).
- [10] J. Jonas, T. DeFries, and D. J. Wilbur, *J. Chem. Phys.* **65**, 581 (1981).
- [11] A. K. Soper and A. Luzar, *J. Phys. Chem.* **100**, 1357 (1996); *J. Chem. Phys.* **97**, 1320 (1992).
- [12] J. E. Bertie and Z. Lan, *Appl. Spectrosc.* **50**, 1047 (1996); J. T. Kindt, and C. A. Schmuttenmaer, *J. Phys. Chem.* **100**, 10373 (1996).
- [13] M. Berg and D. A. Vanden Bout, *Acc. Chem. Res.* **30**, 65 (1997).
- [14] S. Palese, L. Schilling, R. J. D. Miller, P. R. Staver, and W. T. Lotshaw, *J. Phys. Chem.* **98**, 6308 (1994); E. W. Castner Jr., Y. J. Chang, Y. C. Chu, and G. E. Walrafen, *J. Chem. Phys.* **103**, 653 (1995); K. Winkler, J. Lindner, H. Bürsing, and P. Vöhringer, *J. Chem. Phys.* **113**, 4674 (2000); C. J. Fecko, J. D. Eaves, and A. Tokmakoff, *J. Chem. Phys.* **117**, 1139 (2002).
- [15] S. Saito and I. Ohmine, *J. Chem. Phys.* **106**, 4889 (1997); I. Ohmine and S. Saito, *Acc. Chem. Res.* **32**, 741 (1999); B. D. Bursulaya and H. J. Kim, *J. Chem. Phys.* **109**, 4911 (1998).
- [16] A. Perry, H. Ahlborn, B. Space, and P. B. Moore, *J. Chem. Phys.* **118**, 8411 (2003).
- [17] A. Rahman and F. H. Stillinger, *J. Chem. Phys.* **55**, 3336 (1971).
- [18] H. J. C. Berendsen, J. R. Grigera, and T. P. Straatsma, *J. Phys. Chem.* **91**, 6269 (1987).
- [19] *The Chemical Physics of Solvation*, edited by R. Dogonadze, E. Kalman, A. Kornyshev, and J. Ulstrup (Elsevier, Amsterdam, 1985), Part A.
- [20] F. O. Raineri, H. Resat, B.-C. Perng, F. Hirata, and H. L. Friedman, *J. Chem. Phys.* **100**, 1477 (1994); H. L. Friedman, F. O. Raineri, F. Hirata, and B.-C. Perng, *J. Stat. Phys.* **78**, 239 (1995).
- [21] M. Neumann, *J. Chem. Phys.* **85**, 1567 (1986).
- [22] W. L. Jorgensen, S. Chandrasekhar, J. D. Madura, R. W. Impey, and M. L. Klein, *J. Chem. Phys.* **79**, 926 (1983).
- [23] P. A. Madden and R. W. Impey, *Chem. Phys. Lett.* **123**, 502 (1986); B. Guillot, *J. Chem. Phys.* **95**, 1543 (1991); B. D. Bursulaya and H. J. Kim, *J. Chem. Phys.* **109**, 4911 (1998).
- [24] D. Martin, H. Hanthall, *Dimethyl Sulfoxide* (Wiley, New York, 1975); J. C. De la Torre, *Ann. N. Y. Acad. Sci.* **411**, 1 (1983); *Biological Actions of Dimethyl Sulfoxide*; New York Academy of Sciences, vol. 243, edited by S. W. Jacob and R. Herschler (New York, 1975).
- [25] I. I. Vaisman and M. L. Berkowitz, *J. Am. Chem. Soc.* **114**, 7889 (1992); A. Luzar and D. Chandler, *J. Chem. Phys.* **98**, 8160 (1993); A. Vishnyakov, A. P. Lyubarsev, and A. Laaksonen, *J. Phys. Chem. A* **105**, 1702 (2001).
- [26] I. A. Borin and M. S. Skaf, *Chem. Phys. Lett.* **296**, 125 (1998); *J. Chem. Phys.* **110**, 6412 (1999).
- [27] K. J. Packer and D. J. Tomlinson, *Trans. Faraday Soc.* **67**, 1302 (1971).
- [28] M. S. Skaf, *J. Phys. Chem. A* **103**, 10719 (1999).
- [29] U. Kaatze, R. Pottel, and M. Schäfer, *J. Phys. Chem.* **93**, 5623 (1989); S. M. Puranik, A. C. Kumbharkhane, and S. C. Mehrotra, *J. Chem. Soc., Faraday Trans.* **88** 433, (1992).
- [30] *Innovations in Supercritical Fluids, Science and Technology*; K. W. Hutchenon and N. R. Foster, ACS Symposium Series 608; (American Chemical Society, Washington DC, 1995); P. B. Balbuena, L. W. Flanagan, K. P. Johnston, and P. J. Rossky, in *Physical Chemistry of Aqueous Systems: Meeting the Needs of Industry*, H. J. White, J. V. Sengers, D. B. Neumann, and J. C. Bellogs, Eds. (Begell House, New York, 1995); C. A. Eckert, B. L. Knutson, and P. G. Debenedetti, *Nature*, **383**, 313 (1996); See also the thematic issue on supercritical fluids, *Chem. Rev.* **99**, 353 (1999).
- [31] S. C. Tucker, *Chem. Rev.* **99**, 391 (1999); G. Goodyear, S. C. Tucker, *J. Chem. Phys.* **111**, 9673 (1999); S. C. Tucker, M. W. Maddox, *J. Phys. Chem. B* **102**, 2437 (1998).
- [32] K. Okada, M. Yao, Y. Hiejima, H. Kohno, and Y. Kajihara, *J. Chem. Phys.* **107**, 9302 (1997); **110**, 3026 (1999).
- [33] M. S. Skaf and D. Laria, *J. Chem. Phys.* **113**, 3499 (2000).
- [34] C. Yang and H. J. Kim, *J. Chem. Phys.* **113**, 6025 (2000).
- [35] For a general overview of the subject see for instance: M. Maroncelli, *J. Mol. Liq.* **57**, 1 (1993); G. R. Fleming and M. H. Cho, *Ann. Rev. Phys. Chem.* **47**, 109 (1996); P. F. Barbara and W. Jarzaba, *Adv. Photochem.* **15**, 1 (1990).

- [36] For reviews emphasizing theoretical aspects see: R. M. Stratt and M. Maroncelli, *J. Phys. Chem.* **100**, 12981 (1996); B. M. Ladanyi and R. M. Stratt, *J. Phys. Chem.* **99**, 2502 (1995); *J. Phys. Chem.* **100**, 1266 (1996); H. L. Friedman, F. O. Raineri, F. Hirata, and B.-C. Perng, *J. Stat. Phys.* **78**, 239 (1995); F. O. Raineri and H. L. Friedman, *Adv. Chem. Phys.* **107**, 81 (1999); B. Bagchi and R. Biswas, *Adv. Chem. Phys.* **109**, 207 (1999).
- [37] M. S. Skaf and B. M. Ladanyi, *J. Phys. Chem.* **100**, 18258 (1996); *J. Molec. Struct. (THEOCHEM)* **335**, 181 (1995); M. S. Skaf, I. A. Borin, and B. M. Ladanyi, *Molec. Eng.* **7**, 457 (1997);
- [38] D. Laria and M. S. Skaf, *J. Chem. Phys.* **111**, 300 (1999).
- [39] L. R. Martins, A. Tamashiro, D. Laria, and M. S. Skaf, *J. Chem. Phys.* **118**, 5955 (2003).
- [40] B. M. Luther and N. E. Levinger, unpublished; B. M. Luther, PhD. Thesis, Colorado State University (2000).
- [41] P. J. Rossky and J. D. Simon, *Nature* **370**, 263 (1994).
- [42] P. J. Rossky, in *Classical and Quantum Dynamics in Condensed Phase Simulations*, edited by B. J. Berne, G. Cicotti, and D. F. Coker (World Scientific, Singapore, 1998), p. 515.
- [43] O. V. Prezhdo and P. J. Rossky, *J. Phys. Chem.* **100**, 17094 (1996).
- [44] B. J. Schwartz and P. J. Rossky, *J. Chem. Phys.* **101**, 6902 (1994); *J. Chem. Phys.* **105**, 6997 (1996).
- [45] C. Y. Yang, K. F. Wong, M. S. Skaf, and P. J. Rossky, *J. Chem. Phys.* **114**, 3598 (2001).
- [46] Gaathon, A.; Czapski, G.; Jortner, J. *J. Chem. Phys.* **58**, 2648 (1972); Jortner, J.; Gaathon, A., *Can. J. Chem.* **55**, 1801 (1977).
- [47] Michael, B. D.; Hart, E. J.; Schmidt, K., *J. Phys. Chem.* **75**, 2798 (1971).
- [48] Wu, G.; Katsumura, Y.; Muroya, Y.; Li, X.; Terada, Y., *Chem. Phys. Lett.* **325**, 351 (2000); *Radiat. Phys. Chem.* **60**, 395 (2001).
- [49] (a) Bartels, D. M.; Cline, J. A.; Jonah, C. D.; Takahashi, K. *Abstract Am. Chem. Soc. Meeting*, 222:263-PHYS, Part 2 (Washington, August, 2001); (b) Cline J. A.; Jonah, C. D.; Bartels, D. M. *The Solvated Electron in Supercritical Water: Spectra, Yields, and Reactions*, Proceedings of the 1st International Symposium in Supercritical Water-cooled Reactors, Design, and Technology – SCR-2000 (Nov. 6-9,2000, Tokyo, Japan); Dimitrijevic, N. M.; Takahashi, K.; Bartels, D. M.; Jonah, C. D., *J. Phys. Chem. A* **105**, 7236 (2001).
- [50] Giraud, V.; Krebs, P., *Chem. Phys. Lett.* **86**, 85 (1982); Krebs, P.; Heintze, M., *J. Chem. Phys.* **76**, 5484 (1982).
- [51] D. Laria and M. S. Skaf, *J. Phys. Chem. A* **106**, 8066 (2002).
- [52] R. A. Farrer and J. T. Fourkas, *Acc. Chem. Res.* **36**, 605 (2003).
- [53] D. McMorro, W. T. Lotshaw, and G. Kenney-Wallace, *IEEE J. Quantum Electron.* **QE-24**, 443 (1988); S. J. Rosenthal, N. F. Scherer, M. Cho, X. Xie, M. E. Schmidt, and G. R. Fleming, in *Ultrafast Phenomena*, edited by J.-L. Martin, A. Migus, G. A. Mourou, and A. H. Zewail (Springer, Berlin, 1993); R. Righini, *Science* **262**, 1386 (1993).
- [54] M. S. Skaf and S. M. Vecchi, *J. Chem. Phys.* **119**, 2181 (2003).
- [55] E. W. Castner, Jr., Y. J. Chang, Y. C. Chu, and G. E. Walrafen, *J. Chem. Phys.* **103**, 653 (1995).
- [56] D. Oxtoby, *Adv. Chem. Phys.* **40**, 1 (1979); P.-O. Westlund and R. M. Lynden-Bell, *Mol. Phys.* **60**, 1189 (1987).
- [57] K. S. Schweizer and D. Chandler, *J. Chem. Phys.* **76**, 2296 (1982); R. F. Loring and S. Mukamel, *J. Chem. Phys.* **83** 2116 (1985).
- [58] M. C. C. Ribeiro, L. F. C. de Oliveira, and P. S. Santos, *Chem. Phys.* **217**, 71 (1997).
- [59] L. R. Martins, P. A. M. Vazquez, and M. S. Skaf, *J. Molec. Struct. (THEOCHEM)* **580**, 137 (2002).
- [60] L. R. Martins, M. C. C. Ribeiro, and M. S. Skaf, *J. Phys. Chem. B* **106**, 5492 (2002).
- [61] G. L. Richmond, *Annu. Rev. Phys. Chem.* **52**, 357 (2001); *Chem. Rev.* **102**, 2693 (2002).
- [62] K. B. Eisenthal, *Chem. Rev.* **96**, 1343 (1996).
- [63] N. H. Moreira, M.Sc. Thesis, State University of Campinas (2002).
- [64] A. Blondel et al., *J. Mol. Biol.* **291**, 101 (1999).
- [65] W. Bourget et al., *Nature* **375**, 377 (1995).
- [66] Y. K. Cheng, P. J. Rossky, *Nature* **392**, 696 (1998).
- [67] L. Martínez, M.Sc. Thesis, State University of Campinas (2003).